This article has been accepted for publication in a future issue of this journal, but has not been fully edited. Content may change prior to final publication. Citation information: DOI 10.1109/TII.2021.3121333, IEEE Transactions on Industrial Informatics

Multi-Carrier Microgrid Operation Model using Stochastic Mixed Integer Linear Programming

Hasan Mehrjerdi, *Senior Member*, *IEEE,* Reza Hemmati, Sajad Mahdavi, Miadreza Shafie-khah, *Senior Member*, *IEEE,* and João P. S. Catalão, *Senior Member*, *IEEE*

***Abstract*—The microgrid operation is addressed in this paper based on a multi-carrier energy hub. Natural gas, electricity, heating, cooling, hydrogen (H_2), carbon dioxide (CO_2), and renewable energies are considered as the energy carriers. The designed microgrid optimizes and utilizes a wide range of resources at the same time including renewables, electrical storage, hybrid storage, heating-cooling storage, electric vehicles (EV) charging station, power to gas (P2G) unit, combined cooling-heating-power (CCHP), and carbon capture-storage (CCS). The purpose is to reduce the environmental pollutions and operating costs. The resilience and flexibility of the energy hub is also improved. Vehicle to grid (V2G) and fully-partial charge models are incorporated for EVs to improve the system resilience and supplying the critical loads following events. Different events are modeled to evaluate the system resilience. The model is expressed as a stochastic mixed integer linear programming (MILP) problem. Both active and reactive powers are modeled. The microgrid is simulated under four different cases. The results show that the multi type energy storages reduce the annual cost of energy while the integrated charging station can decrease the load shedding.**[1]

Index Terms*—*Electric Vehicle Charging Station, CO_2 Trading, Multi Type Energy Storage, Power to Gas, Resilience.

I. Nomenclature

Indexes and Sets	
ac, ec, bo, sw, we, cap	Index of absorption and electric chillers, boiler, solar water heater, water electrolyzer and supercapacitor
es, cs, hs, gs, CO_2s	Index of energy, cooling, heating, gas and CO_2 storages
f, F	Index of faults, set of faults
kl, KL	Index of loads, set of loads
k,K	Index of polygon lines, set of polygon lines
s,S	Index of scenarios, set of scenarios
se, SE	Index of seasons, set of seasons
t, T	Index of time intervals, set of time intervals
vn, VN	Index of vehicle, set of vehicles
Parameters	
α, β^{-1}	Conversion factor of CO_2 and natural gas (kg/MWh)
BM	Big-M coefficient
Cap_{vn}	Electric vehicle capacity (MWh)
COP_{cs}, COP_{ac}, COP_{ec}	Coefficient of performance of cooling storage, absorption and electric chiller
$\boldsymbol{DS_{se}^{f}}$	Number of fault days in each season
DRP_{up}, DRP_{down}	Added or deducted active demand for shiftable loads (MW)
E^{ini}, E^{max}, E^{min}	Initial, max and min energy of storage (MWh)
FR^{max}, FR^{min}	Maximum and minimum flow rate (kg/h)
$\boldsymbol{H_{bo}^{max}}$	Maximum heating power of boiler (MW)
I_t, I_{STC}	solar radiation intensity, irradiance intensity at standard condition
$\boldsymbol{L_{ea}}$, $\boldsymbol{L_c}$, $\boldsymbol{L_h}$, $\boldsymbol{L_{com}}$	Electrical, cooling, heating, combinational loads (MW)
$\boldsymbol{L_{er}}$	Electrical reactive load (MVar)
M^{ini}, M^{max}, M^{min}	Initial, maximum and minimum stored mass (kg)
pr_{drp}	Cost coefficient of active shifted power
P_{sell}	price of selling CO_2 (\$/kg)
$\boldsymbol{P_{pin}^{se,t}}$, $\boldsymbol{P_{gin}^{se,t}}$	Price of purchased active power, natural gas (\$/MWh)
P_{CO2}	Price of CO_2 emission (\$/kg)
$\boldsymbol{p_{qin}^{se,t}}$	Price of purchased reactive power, (\$/MVarh)
P_{pv}, P_w	Power of photovoltaic and wind units (MW)
$\boldsymbol{P_{ch}^{max}}$, $\boldsymbol{P_{dis}^{max}}$	Maximum active power for charging and discharging of battery, heating and cooling storage (MW)
P_{STC}	Rated power of PV panel (MW)
Pro	Scenario probability
P_r	Rated output power (MW)
P_{st}, P_{sh}	Start-up and shut-down price of CHP (\$)
$\boldsymbol{P_{vn}^{max}}$	Maximum power of EV (MW)
$\boldsymbol{Q_{es}^{max}}$	Maximum reactive power for battery (MVar)
S_{chp}^{A}	Apparent power of CHP(MVA)
T_t	Ambient temperature (°C)
υ_t, υ_{in}, υ_{out}, υ_r	Wind speed, cut in and cut out speeds, rated speed (m/s)
ξ_p	Penalty coefficient
$\boldsymbol{\delta_{es}^{self}}$	Self-discharge of battery (%)
$\boldsymbol{\eta_{es}^{ch}}$, η_{es}^{dis}	Charging and discharging efficiency of battery (%)
η_p^{chp}, η_h^{chp}, η_h^{bo}	Electrical and heating efficiency of CHP and boiler (%)
η_{in}	Conversion efficiency of PV inverter
γ	Shiftable load factor
Δt	Duration of time interval (hour)
Binary variables	
u, x, y	Auxiliary variable for modelling the storages, CHP, supercapacitor
z	Auxiliary variable for modelling EV charging station
Continuous variables	
C_{Pin}, C_{Qin}	Cost of purchased active and reactive powers (\$/year)
C_{Gin}, C_{CO2}	Cost of purchased natural gas, CO2 emission (\$/year)
$C_{chp}^{st\ \&\ sh}$	Start-up and shut-down annual cost of CHP (\$/year)
C_{shed}^{p}, C_{EV}^{p}	Penalty cost of load shedding and EV partial charge (\$/year)
$C_{shed}^{kl,se,f,s,t}$	Penalty cost of load shedding (\$)
$C_{vn}^{se,f,t}$	Penalty cost to EV partial charge (\$)
C_{sell}	Revenue of selling CO2 (\$)
$C_{st}^{se,f,t}$, $C_{sh}^{se,f,t}$	Start-up and shut down cost of CHP in season se, fault f and time slot t (\$)
C_{DR}	Incentive cost for shiftable loads in DRP (\$/year)
$CO2^{se,f,s,t}$, $G_{in}^{se,f,t}$	CO_2 emission and input natural gas (kg/h)
$CO2_{chp\ \&\ bo}^{se,f,s,t}$	CO_2 produced by CHP and boiler (kg/h)
$CO2_{cap}^{se,f,s,t}$	Captured CO_2 from CHP and boiler (kg/h)
$CO2_{P2G}^{se,f,s,t}$	Input flow rate of CO_2 into P2G unit (kg/h)
$C_{se}^{se,f,s,t}$, $C_{ac}^{se,f,s,t}$	Generated cooling power by electric and absorption chillers (MW)
$C_{cs,ch}^{se,f,t}$, $C_{cs,dis}^{se,f,t}$	Charging and discharging cooling power of cooling storage tank (MW)
$E_{\boldsymbol{vn}}^{se,f,t}$, $E_{vn}^{se,f,tleave}$	Stored energy in time slot t and leaving time from station (MWh)
$E_{es}^{se,f,t}$, $E_{cap}^{se,f,s,t}$	Stored energy in battery and supercapacitor (MWh)
FR_{CO2s}, FR_{gS}	Flow rate of CO_2 and natural gas storage tanks (kg/h)
$FR_{sell}^{se,f,s,t}$	CO_2 selling (kg/h)
$FR_{H2}^{se,f,s,t}$, $G_{P2G}^{se,f,s,t}$	Flow rate of H_2 and natural gas regeneration (kg/h)
$H_{chp}^{se,f,t}$, $H_{bo}^{se,f,s,t}$	Heating power of CHP and boiler (MW)
$H_{ac}^{se,f,s,t}$, $H_{sw}^{se,f,s,t}$	Generated heating by absorption chiller and solar water heater (MW)
$H_{com}^{se,f,s,t}$	Heating power of combinational load (MW)
$H_{hs,ch}^{se,f,t}$, $H_{hs,dis}^{se,f,t}$	Charging and discharging heating power of heating storage tank (MW)
$M_{CO2s}^{se,f,t}$, $M_{gs}^{se,f,t}$	Stored CO_2 and natural gas in storage tanks (kg)
$\boldsymbol{P}_{in}^{se,f,s,t}$, $Q_{\boldsymbol{in}}^{se,f,s,t}$	Input active (MW) and reactive (MVar) power
$P_{chp}^{se,f,t}$, $H_{chp}^{se,f,t}$	Active power and heating generated by CHP (MW)
$P_{cs}^{se,f,t}$	The electrical power consumed by cooling storage (MW)
$P_{cs,ch}^{se,f,t}$, $P_{cs,dis}^{se,f,t}$	The electrical power for ice making ad melting by cooling storage (MW)

Corresponding authors: M. Shafie-khah; J.P.S. Catalão.
H. Mehrjerdi is with the Electrical Engineering Department, Qatar University, Doha, Qatar (hasan.mehrjerdi@qu.edu.qa)
R. Hemmati and S. Mahdavi are with the Department of Electrical Engineering, Kermanshah University of Technology, Kermanshah, Iran (r.hemmati@kut.ac.ir; smahdavik@gmail.com)
M. Shafie-khah is with the School of Technology and Innovation, University of Vaasa, Vaasa, Finland (e-mail: miadreza.shafiekhah@uva.fi).
J.P.S. Catalão is with the Faculty of Engineering of the University of Porto and INESC TEC, Porto 4200-465, Portugal (e-mail: catalao@fe.up.pt).

This article has been accepted for publication in a future issue of this journal, but has not been fully edited. Content may change prior to final publication. Citation information: DOI 10.1109/TII.2021.3121333, IEEE Transactions on Industrial Informatics

$H_{bo}^{se,f,s,t}$	Heating power produced by CHP (MW)
$P_{es,ch}^{se,f,t}$, $P_{es,dis}^{se,f,t}$	Active power exchange of battery storage (MW)
$P_{cap}^{se,f,s,t}$, $P_{vn}^{se,f,t}$	Active power of supercapacitor and electric vehicle (MW)
$P_{\mathbf{com}}^{se,f,s,t}$, $P_{ec}^{se,f,s,t}$	Input power of combinational load and electric chiller (MW)
$P_{we}^{se,f,s,t}$, $P_{cs}^{se,f,t}$	Input power of water electrolyzer and cooling storage tank (MW)
P_{DR}	New active loads after DRP (MW)
$Q_{in}^{se,f,s,t}$, $Q_{chp}^{se,f,t}$	Reactive power of electrical network, CHP(MVar)
$Q_{es}^{se,f,t}$	Reactive power of battery storage (MVar)
$\Omega_{kl}^{se,f,s,t}$, $\psi_{vn}^{se,f,t}$	Amount of supplied load and EV charge (%)

II. Introduction

A. Motivations of this work

Nowadays, growing concerns about environmental and energy issues are encouraging efficient energy production and consumption systems. With respect to the energy efficiency and resilience, the integrated energy systems composed of electrical, gas and heating networks are attracting more attention. The multi-carrier energy (MCE) systems directly influence the security and economic operation aspects of power systems. For example, the combined cooling, heating and power (CCHP) enables the users to utilize multiple energies with about 60-80% efficiency. The CCHP can reduce the pollutants produced by the conventional fossil fuel power plants [1]. The plug-in electric vehicles (PEVs) can also play a significant role in reducing the petrol consumption and operating costs, improving reliability and supplying the loads following outages in order to improving the resilience [2]. The resilience shows the capability of the network to operate under extreme conditions caused by weather and natural disasters [3]. The above-mentioned items have motivated the authors to consider a multi carried energy hub for microgrid resilience and operation.

B. Literature Survey and Contributions

The MCE systems have been investigated from different viewpoints such as topology of energy hubs, types of energy storages, combined effects of component, environmental impacts, carbon emission reduction strategies, and robust-resilience operation. In MCE, the energy hub is an interface between different energy systems playing the role of energy production, conversion and storage [4]. Moreover, energy hub is a multi input/output unit and has the capability of assisting the energy management and optimization by combining and coupling multiple energy carriers [5].

The electricity, heating, cooling and combinational hubs are the main energy hubs in such systems [4]. As well, some key components and sectors used in MCE systems are: thermal devices, multi type energy storages, combined heat and power, renewable resources, boilers, plug in electric vehicles and the charging stations. The heat energy storage is attracting interest due to the its high efficiency, large capacity and low cost [6]. The hybrid energy storage and plug in electric vehicle can return the stored energy to the hub in order to supplying the electrical appliances whenever needed. This can effectively improve the efficiency of renewables [7, 8].

The MCE systems have been extensively recognized as an efficient way of reducing carbon emission by promoting the integration of renewable energies [9]. The Carbon tax policy [9], carbon emission caps [10], carbon emission trading [11], carbon capture and storage [12], methanation reaction and Power-to-Gas (P2G) technology [13] are the most popular methods in the reduction of carbon emission. The rapid development of P2G technology in recent years has enabled on-site capture and recycling of CO_2 using surplus of renewable energies [14, 15]. One of the best advantages of the combined MCE-P2G system is the on-site recycling of CO_2 and reducing the carbon emission without long-distance transportation of CO_2. The other important issue that can be dealt with the MCE hubs is the resilience. The MCE systems are proper facilities to improve the system resilience. The extreme weather events have increasingly affected power systems worldwide. The global attention to catastrophic consequences of such high impact rare events has promoted the concept of power system resilience [16]. With respect to the above discussed items, it is concluded that various studies have been published about application of different energy carriers (electricity, gas, hydrogen, etc.) and various technologies (renewable, EV, storage, etc.) in the MCE hub. Moreover, various concepts such as resilience, CO_2 reduction, and robust operation have already been discussed. But none of them considered all of these subjects together in one model. This point is addressed in Table I.

In order to address such research gaps, this paper presents a resilient comprehensive model for microgrid operation based on multi-carrier energy hub including electricity, gas, heating, cooling, hydrogen, methane, and CO_2. In actual, each of loads is supplied through different parallel paths that increases the system resilience. As well, the model utilizes various technologies including hybrid electrical storage, thermal storage, renewables, EV charging station, P2G, CCHP, and carbon capture-storage. The model enhances the system resilience by supplying the loads through various paths, minimizes CO_2 emission by capturing/ selling and using carbon and reduces the operating cost.

The main contributions of the given model are summarized as follows:

- The model includes various energy carriers including electricity, natural gas, heating, cooling, hydrogen and CO_2; thus, all of the loads are supplied multidirectionally.
- The model utilizes many equipment comprising hybrid storage, thermal storage, renewables, EV charging station, P2G, CCHP, carbon capture and storage, boiler, absorption chiller, and electrical chiller. Each equipment deals with one or more energy carrier.
- The partial charge capability is carried out for electric vehicles in order to supply the critical loads under faulty condition.
- The CO2 generated by CHP and boiler is captured and used for selling, monetization and natural gas regeneration in the P2G unit.
- The optimal operation pattern is scheduled for all equipment and both active/reactive powers are incorporated.
- Uncertainty of loads and renewables (e.g., solar PV, wind, solar water heater) are modeled.
- The model aims to enhance the system resilience, minimize CO_2 emissions and reduce the operating costs.

The main contributions of current research against the previous ones are listed in Table I.

III. Proposed framework description

A. Multi-carrier energy systems

MCE system can be modeled with the energy hub concept which is considered as a unit where multiple energy carriers can be converted, stored and distributed. The MCE system can have multiple input and output ports, the input ports are usually connected to electricity, natural gas, district heat or other types of energy, while the output ports can provide power, heat, cool, natural gas, and multi energy services simultaneously.

The management strategy in a typical MCE system is shown by Fig. 1. The input energies of this system are supplied by electrical and gas networks and the outputs are electrical, cooling, heating, and combinational loads. The interaction between different energy carriers through the main energy converters (C1 to C6) is shown by Fig. 2. The converters C1 and C2 consume the electricity and heating, respectively, and produce cooling energy. The generated cooling is appropriate with their coefficient of performance. These converters are known as electrical and absorption chillers. The converters C3 and C4 (i.e., CHP and boiler) consume natural gas in order to generate electricity and heating simultaneously. The C5 is a water electrolyzer that consumes electricity and produces hydrogen. In C6, the released CO2 by CHP and boiler is combined with hydrogen to produce the natural gas. This converter is the methanation unit. Combination of C5 and C6 is named P2G unit.

B. Carbon capture storage and natural gas recycle

Carbon capture and storage is one of the important methods for environmental pollution reduction. This technology consists of three units including capture unit, compression unit and storage tank. In order to generating the natural gas, carbon capture unit delivers CO_2 to P2G unit. The P2G unit consists of two units including water electrolyze and methanation units. The P2G uses CO_2 and hydrogen to produce methane (natural gas).

TABLE I: Comparing the current paper with the literature

		Demand type	Storage type	CHP modelling	EV charging station	CO_2 reduction	The other items
Ref. No	Year	Electrical+ Heat+ cooling+ combinational (E&H)	ES+HS+CS +GS+CO_2S	YES	YES	P2G system + emission cost	Resilience analysis under natural gas interruption, islanding mode and hurricane landfall events+ Penalty cost of load shedding
[17]	2018	Electrical+ Heat	ES+GS+HS	NO	NO	NO	NO
[18]	2019	Electrical+ Heat+ cooling	ES	NO	NO	NO	NO
[3]	2018	Electrical+ Gas	GS	NO	NO	NO	load shedding cost to enhancement of resilience
[4]	2018	Electrical+ Heat	ES+HS	NO	NO	NO	NO
[5]	2018	Electrical+ Heat	ES+HS	NO	NO	NO	NO
[19]	2018	Electrical+ Heat+ cooling	ES+HS	NO	NO	Emission cost	NO
[20]	2019	Electrical+ Heat+ combinational (E&H)	ES+HS	YES	NO	NO	Resilience analysis under islanding mode + optimization of load shedding cost
[9]	2019	Electrical+ Heat+ cooling	CS+HS	NO	NO	Carbon tax	NO
[21]	2018	Electrical+ Heat+ cooling	ES+HS+CS+ GS	NO	NO	P2G system + carbon tax	NO
[15]	2017	Electrical+ Heat+ Gas	ES+HS+GS	NO	NO	P2G system + emission cost	NO
[22]	2018	Electrical+ Heat	CO_2S+GS	NO	NO	P2G system	NO
[23]	2018	Electrical+ Heat	Electrical+ Heat	NO	NO	NO	Resilience analysis under natural gas interruption, islanding mode and hurricane landfall event
Current paper	-------	Electrical+ Heat+ cooling+ combinational (E&H)	ES+HS+CS +GS+CO_2S	YES	YES	P2G system + emission cost	Resilience analysis under natural gas interruption, islanding mode and hurricane landfall events+ Penalty cost of load shedding

The models given by literature (ES=battery energy storage, GS= natural gas storage, HS= heating storage, CS= cooling storage, CO_2S= CO_2 storage)

C. Resilience and system faults

A typical resilience curve for a given measure of performance (MoP) associated with an extreme event is shown by Fig. 3. All of the processes from pre-fault, recovery and post-fault are expressed in the figure. Once the fault occurs (t_f) in the network, the system performance starts to degradation and its intensity depends on the fault type and location. The ability of network to supply the critical loads under events is assumed as network robustness. In this paper multiple and different types of faults are imposed on the network to evaluate the resilience and robustness of the model. The electrical network outage, natural gas network outage, earthquake event and destruction of solar and wind units, outage of CHP and outage of boiler are considered for network resilience assessment.

D. The proposed microgrid based on MCE

Fig. 4 shows the proposed microgrid based on MCE system. This model is very complex which increases the costs on the one hand and improves the resilience and reliability on the other hand. The model may also be simplified to have the grids with less cost as well as less resilience and reliability. It often depends on the importance and priority of the loads to select the topology of the grid. The electricity and natural gas are main inputs to the microgrid and the electrical, combinational, cooling-heating loads are the outputs. The microgrid can sell active power to the network. The reactive power of microgrid is supplied by the electrical network, hybrid battery-capacitor storage and CHP. The renewables are solar PV, solar water heater and wind units. Multi type energy storages are considered to enhance the flexibility and reliability. These storages are hybrid battery-capacitor, heating-cooling, CO_2 and natural gas storage. The performance of these energy storages is on different energy carriers, for this reason, the operation of them under small load variations is independent of each other. As a result, it is not efficient to replace all of these small storage units with one large-scale storage system which is installed on one of the energy carriers.

The hybrid energy storage can absorb the stochastic behavior of renewable energies. The natural gas storage has an important role for supplying gas when the input gas pipeline is not available.

Fig. 1: Management strategy in a typical MCE system

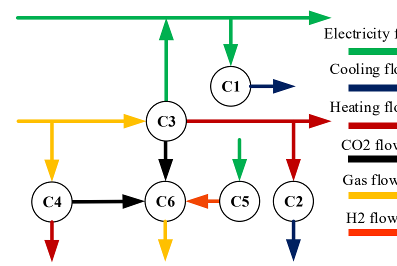

Fig. 2: Interactions between different energy carriers through energy converters

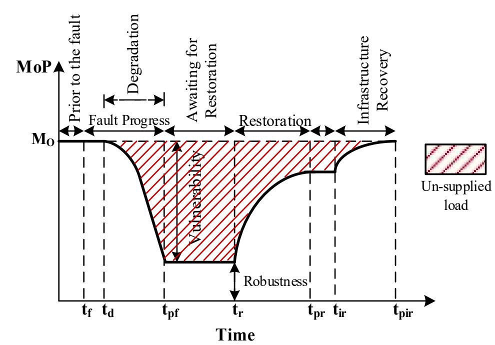

Fig. 3: A typical resilience curve [16]

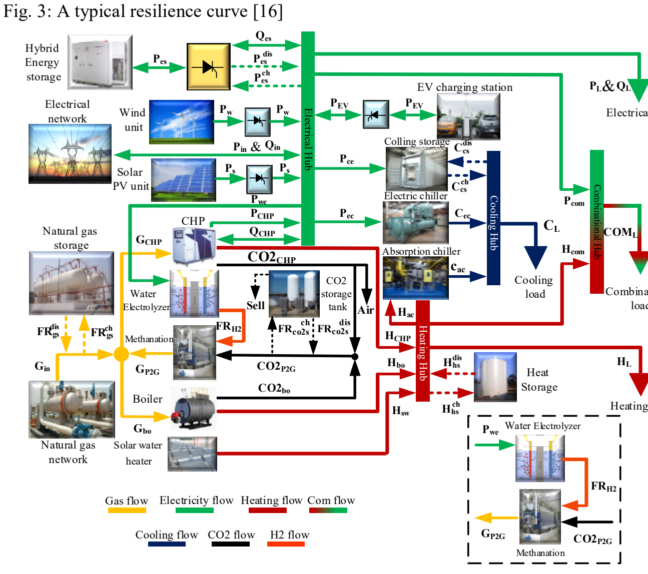

Fig. 4: The proposed microgrid based on MCE

This article has been accepted for publication in a future issue of this journal, but has not been fully edited. Content may change prior to final publication. Citation information: DOI 10.1109/TII.2021.3121333, IEEE Transactions on Industrial Informatics

The CHP and boiler are the heating resources and the electrical and absorption chillers are the cooling resources. The cooling storage works based on ice making and melting mechanism. The generated CO_2 by CHP and boiler can be released into the air, sold, stored or it may be used for natural gas regeneration in P2G unit. The P2G comprises the water electrolyzer for H_2 generation and Methanation units for producing Methane gas (CH_4). The EVs charging station is also considered with capability of fully-partial charge operation.

IV. Problem Formulation

A. Objective function

The objective function of the problem is the annual operating cost that is shown by (1) that is summation of purchased active and reactive power costs, purchased gas cost, CO_2 emission cost, load shedding cost, penalty cost of EV partial charge and cost of CHP start up-shut down minus the revenue achieved from CO_2 selling. These items are listed through (2) to (11), respectively. Start-up and shut down cost of CHP in season is linearized by (12) [20] and details of equations (7) and (8) are expressed by (13) and (14).

$$OF = C_{Pin} + C_{Qin} + C_{Gin} + C_{CO2} + C_{CHP}^{st\&sh} + C_{shed}^{p} + C_{EV}^{p} - C_{sell}^{co2} \tag{1}$$

$$C_{Pin} = \sum_{se=1}^{SE}\left(\sum_{f=1}^{F} D_{se}^{f}\left(\sum_{s=1}^{S}\left[\sum_{t=1}^{T} P_{in}^{se,f,s,t}.\Delta t.p_{pin}^{se,t}\right]\mathrm{Pro}^{s}\right)\right) \tag{2}$$

$$C_{Qin} = \sum_{se=1}^{SE}\left(\sum_{f=1}^{F} D_{se}^{f}\left(\sum_{s=1}^{S}\left[\sum_{t=1}^{T} Q_{in}^{se,f,s,t}.\Delta t.p_{qin}^{se,t}\right]\mathrm{Pro}^{s}\right)\right) \tag{3}$$

$$C_{Gin} = \sum_{se=1}^{SE}\left(\sum_{f=1}^{F} D_{se}^{f}\left(\sum_{s=1}^{S}\left[\sum_{t=1}^{T} G_{in}^{se,f,s,t}.\beta.\Delta t.p_{gin}^{se,t}\right]\mathrm{Pro}^{s}\right)\right) \tag{4}$$

$$C_{CO2} = \sum_{se=1}^{SE}\left(\sum_{f=1}^{F} D_{se}^{f}\left(\sum_{s=1}^{S}\left[\sum_{t=1}^{T} CO2^{se,f,s,t}.\Delta t.p_{co2}\right]\mathrm{Pro}^{s}\right)\right) \tag{5}$$

$$C_{CHP}^{st\&sh} = \sum_{se=1}^{SE}\left(\sum_{f=1}^{F} D_{se}^{f}\left(\sum_{t=1}^{T} C_{st}^{se,f,t} + C_{sh}^{se,f,t}\right)\right) \tag{6}$$

$$C_{shed}^{p} = \sum_{kl}^{KL}\left(\sum_{se=1}^{SE}\left(\sum_{f=1}^{F} D_{se}^{f}\left(\sum_{s=1}^{S}\sum_{t=1}^{T} C_{shed}^{kl,se,f,s,t}.\mathrm{Pro}^{s}\right)\right)\right) \tag{7}$$

$$C_{EV}^{p} = \sum_{se=1}^{SE}\left(\sum_{f=1}^{F} D_{se}^{f}\left(\sum_{t=1}^{T}\left(\sum_{vn=1}^{VN} C_{vn}^{se,f,t}\right)\right)\right) \tag{8}$$

$$C_{sell} = \sum_{se=1}^{SE}\left(\sum_{f=1}^{F} D_{se}^{f}\left(\sum_{s=1}^{S}\left[\sum_{t=1}^{T} FR_{sell}^{se,f,s,t}.\Delta t.p_{sell}\right]\mathrm{Pro}^{s}\right)\right) \tag{9}$$

$$CO2^{se,f,s,t} = CO2_{chp\&bo}^{se,f,s,t} - \left(CO2_{P2G}^{se,f,s,t} + FR_{co2s}^{se,f,s,t}\right) \tag{10}$$

$$CO2_{chp\&bo}^{se,f,s,t} = \left(P_{chp}^{se,f,t}/\eta_{P}^{chp} + H_{chp}^{se,f,t}/\eta_{H}^{chp} + H_{bo}^{se,f,s,t}/\eta_{H}^{bo}\right).\alpha \tag{11}$$

$$\begin{cases} C_{sh}^{se,f,t} \ge P_{sh}.(x^{se,f,t-1} - x^{se,f,t}) & \forall t \ne 1 \\ C_{st}^{se,f,t} \ge P_{st}.(x^{se,f,t} - x^{se,f,t-1}) & \forall t \ne 1 \\ C_{sh}^{se,f,t} \ge P_{sh}.(x^{se,f,T} - x^{se,f,t}) & \forall t = 1 \\ C_{st}^{se,f,t} \ge P_{st}.(x^{se,f,t} - x^{se,f,T}) & \forall t = 1 \end{cases} \tag{12}$$

$$C_{shed}^{kl,se,f,s,t} = (1-\Omega_{kl}^{se,f,s,t}).L_{kl}^{se,s,t}.\Delta t.\xi_{p}.p_{pin}^{se,t} \tag{13}$$

$$C_{vn}^{se,f,t} = (1-\psi_{vn}^{se,f,t}).cap_{vn}.\xi_{p}.p_{pin}^{se,t} \tag{14}$$

B. Power balance constraints in energy hubs

The power balance constraints related to electrical, heating, cooling and combinational hubs for faulty time periods (f≠1) and the other time intervals (healthy periods) (f=1) is expressed through (15) to (20). It is noteworthy that the suppling the load must always be greater than the critical load, where (1-Ω) is expressed as percentage of un-supplied load. The electrical hub is modeled by (15) and (16).

$$\begin{cases} P_{in}^{se,f,s,t} + P_{pv}^{se,f,s,t} + P_{w}^{se,f,s,t} + P_{chp}^{se,f,t} + P_{cap}^{se,f,s,t} + P_{es,dis}^{se,f,t} - P_{es,ch}^{se,f,t} \\ -\sum_{vn=1}^{VN} P_{vn}^{se,f,t} - P_{com}^{se,f,s,t} - P_{ec}^{se,f,s,t} - P_{we}^{se,f,s,t} - P_{cs}^{se,f,t} \\ \begin{cases} \ge \Omega_{a}^{se,f,s,t}.L_{ea}^{se,s,t} & \forall f \ne 1 \\ = L_{ea}^{se,s,t} & \forall f = 1 \end{cases} \end{cases} \tag{15}$$

$$Q_{in}^{se,f,s,t} - Q_{chp}^{se,f,t} - Q_{es}^{se,f,t} \begin{cases} \ge \Omega ea^{se,f,s,t}.L_{er}^{se,s,t} & \forall f \ne 1 \\ = L_{er}^{se,s,t} & \forall f = 1 \end{cases} \tag{16}$$

The heating hub is modeled by (17) and cooling is specified in (18).

$$\begin{aligned} &H_{chp}^{se,f,t} + H_{bo}^{se,f,s,t} + H_{sw}^{se,f,s,t} + H_{hs,dis}^{se,f,t} - H_{hs,ch}^{se,f,t} - \\ &H_{ac}^{se,f,s,t} - H_{com}^{se,f,s,t} \begin{cases} \ge \Omega_{h}^{se,f,s,t}.L_{h}^{se,s,t} & \forall f \ne 1 \\ = L_{h}^{se,s,t} & \forall f = 1 \end{cases} \end{aligned} \tag{17}$$

$$C_{ec}^{se,f,s,t} + C_{ac}^{se,f,s,t} + C_{cs,dis}^{se,f,t} - C_{cs,ch}^{se,f,t} \begin{cases} \ge \Omega_{c}^{se,f,s,t}.L_{c}^{se,s,t} & \forall f \ne 1 \\ = L_{c}^{se,s,t} & \forall f = 1 \end{cases} \tag{18}$$

The combinational hub is defined in (19).

$$P_{com}^{se,f,s,t} + H_{com}^{se,f,s,t} \begin{cases} \ge \Omega_{com}^{se,f,s,t}.L_{com}^{se,s,t} & \forall f \ne 1 \\ = L_{com}^{se,s,t} & \forall f = 1 \end{cases} \tag{19}$$

C. CHP modelling

The typical feasible operation region of CHP unit is shown by Fig. 5 that can be formulated by the set of linear equations (20) to (25) [20], when x=0, the output apparent electrical power and heat of the CHP unit are zero. Meanwhile, the apparent power of CHP is limited by (26). In order to linearizing this constraint, the hexagon approximations of a circle used and expressed by (27) [24].

$$P_{chp}^{se,f,t} - P_{chp}^{A} - \frac{P_{chp}^{A} - P_{chp}^{B}}{H_{chp}^{A} - H_{chp}^{B}}\left(H_{chp}^{se,f,t} - H_{chp}^{A}\right) \le 0 \tag{20}$$

$$P_{chp}^{se,f,t} - P_{chp}^{B} - \frac{P_{chp}^{B} - P_{chp}^{C}}{H_{chp}^{B} - H_{chp}^{C}}\left(H_{chp}^{se,f,t} - H_{chp}^{C}\right) \ge -\left(1 - x^{se,f,t}\right).BM \tag{21}$$

$$P_{chp}^{se,f,t} - P_{chp}^{C} - \frac{P_{chp}^{C} - P_{chp}^{D}}{H_{chp}^{C} - H_{chp}^{D}}\left(H_{chp}^{se,f,t} - H_{chp}^{D}\right) \ge -\left(1 - x^{se,f,t}\right).BM \tag{22}$$

$$0 \le H_{chp}^{se,f,t} \le H_{chp}^{B}.x^{se,f,t} \tag{23}$$

$$0 \le P_{chp}^{se,f,t} \le P_{chp}^{A}.x^{se,f,t} \tag{24}$$

$$0 \le S_{chp}^{se,f,t} \le S_{chp}^{A}.x^{se,f,t} \tag{25}$$

$$(P_{chp}^{se,f,t})^2 + (Q_{chp}^{se,f,t})^2 \le (S_{chp}^{A})^2 \tag{26}$$

$$P_{chp}^{se,f,t}.\cos\frac{(2k-1)}{K}\pi + Q_{chp}^{se,f,t}.\sin\frac{(2k-1)}{K}\pi - S_{chp}^{A}.\cos\frac{\pi}{K} \le 0 \tag{27}$$

D. Chiller and boiler constraints

The electric and absorption chillers consume electricity and heat and produce cooling power. The relationship between input and output powers of these components are indicated by (28)-(29) [25]. The output heating power of boiler is limited by (30) [25].

$$C_{ec}^{se,f,s,t} = P_{ec}^{se,f,s,t}.COP_{ec} \tag{28}$$

$$C_{ac}^{se,f,s,t} = H_{ac}^{se,f,s,t}.COP_{ac} \tag{29}$$

$$0 \le H_{bo}^{se,f,s,t} \le H_{bo}^{\max} \tag{30}$$

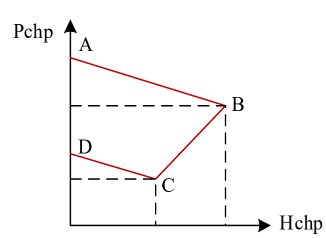

Fig. 5: A typical feasible operation region of a CHP unit

This article has been accepted for publication in a future issue of this journal, but has not been fully edited. Content may change prior to final publication. Citation information: DOI 10.1109/TII.2021.3121333, IEEE Transactions on Industrial Informatics

E. Energy storages devices constraints

1) Hybrid, heating and cooling energy storages

The hybrid energy storage can therefore absorb the stochastic behavior of renewable energies. The supercapacitor operation is modeled by (31)-(35). The battery energy storage behavior is modelled by (36)-(42), where (42) shows the reactive power absorption or injection by battery [25]. The cooling and heating storage constraints are similar to (36)-(41) and the similar operation is modeled for them. The electrical power to ice making or melting (charging and discharging) is expressed by (43) and equations (44)-(45) represent the output cooling power of ice storage [25].

$$P_{cap}^{se,f,s,t} = y_c^{se,f,s,t} . \left((P_{pv}^{se,f,s1,t} + P_w^{se,f,s1,t}) - (P_{pv}^{se,f,s,t} + P_w^{se,f,s,t}) \right) \tag{31}$$

$$E_{cap}^{se,f,s,t} = E_{cap}^{ini} + P_{cap}^{se,f,s,t} .\Delta t \quad \forall t = 1 \tag{32}$$

$$E_{cap}^{se,f,s,t} = E_{cap}^{se,f,s,t-1} + P_{cap}^{se,f,s,t} .\Delta t \quad \forall t \neq 1 \tag{33}$$

$$E_{cap}^{se,f,s,T} = E_{cap}^{ini} \tag{34}$$

$$E_{cap}^{\min} \leq E_{cap}^{se,f,s,t} \leq E_{cap}^{\max} \tag{35}$$

$$E_{es}^{se,f,t} = E_{es}^{ini} (1-\delta_{es}^{self}) + (P_{es,ch}^{se,f,t} .\eta_{es}^{ch} - P_{es,dis}^{se,f,t} / \eta_{es}^{dis}) \Delta t \ \forall t = 1 \tag{36}$$

$$E_{es}^{se,f,t} = E_{es}^{se,f,t-1} (1-\delta_{es}^{self}) + (P_{es,ch}^{se,f,t} .\eta_{es}^{ch} - P_{es,dis}^{se,f,t} / \eta_{es}^{dis}) \Delta t \quad \forall t \neq 1 \tag{37}$$

$$E_{es}^{se,f,T} = E_{es}^{ini} \tag{38}$$

$$E_{es}^{\min} \leq E_{es}^{se,f,t} \leq E_{es}^{\max} \tag{39}$$

$$0 \leq P_{es,ch}^{se,f,t} \leq P_{es,ch}^{\max} . u_{es}^{se,f,t} \tag{40}$$

$$0 \leq P_{es,dis}^{se,f,t} \leq P_{es,dis}^{\max} \cdot (1 - u_{es}^{se,f,t}) \tag{41}$$

$$-Q_{es}^{\max} u_{es}^{se,f,t} \leq Q_{es}^{se,f,t} \leq Q_{es}^{\max} u_{es}^{se,f,t} \tag{42}$$

$$P_{cs}^{se,f,t} = P_{cs,ch}^{se,f,t} + P_{cs,dis}^{se,f,t} \tag{43}$$

$$C_{cs,ch}^{se,f,t} = P_{cs,ch}^{se,f,t} .COP_{cs} \tag{44}$$

$$C_{cs,dis}^{se,f,t} = P_{cs,dis}^{se,f,t} .COP_{cs} \tag{45}$$

2) CO_2 storage constraints

The produced CO_2 by CHP and boiler can be stored in CO_2 storage tank and it can be used by P2G unit in order to recycling the natural gas. Behavior of this storage is modelled by (46) - (50).

$$M_{co2s}^{se,f,s,t} = M_{co2s}^{ini} + (FR_{co2}^{se,f,s,t} - FR_{sell}^{se,f,s,t}).\Delta t \quad \forall t = 1 \tag{46}$$

$$M_{co2s}^{se,f,s,t} = M_{co2s}^{se,f,s,t-1} + (FR_{co2s}^{se,f,s,t} - FR_{sell}^{se,f,s,t}).\Delta t \ \forall t \neq 1 \tag{47}$$

$$M_{co2s}^{se,f,s,T} = M_{co2s}^{ini} \tag{48}$$

$$-M .FR_{co2s}^{\max} \leq FR_{co2s}^{se,f,s,t} .\Delta t \leq FR_{co2s}^{\max} .BM \tag{49}$$

$$M_{co2s}^{\min} \leq M_{co2s}^{se,f,s,t} \leq M_{co2s}^{\max} \tag{50}$$

3) Natural gas storage constraints

The natural gas storage tank has an important role to system gas supply when the input natural gas from natural gas network is cut off. Equations (51)-(54) show natural gas storage tank constraints.

$$M_{gs}^{se,f,t} = M_{gs}^{ini} + FR_{gs}^{se,f,t} .\Delta t \qquad \forall t = 1 \tag{51}$$

$$M_{gs}^{se,f,t} = M_{gs}^{se,f,t-1} + FR_{gs}^{se,f,t} .\Delta t \quad \forall t \neq 1 \tag{52}$$

$$M_{gs}^{se,f,T} = M_{gs}^{ini} \tag{53}$$

$$-BM .FR_{gs}^{\max} \leq FR_{gs}^{se,f,t} \leq FR_{gs}^{\max} .BM \tag{54}$$

$$M_{gs}^{\min} \leq M_{gs}^{se,f,t} \leq M_{gs}^{\max} \tag{55}$$

F. P2G modelling

The CO_2 balance constraint is expressed by (56). The captured CO_2 is smaller or equal to produced CO_2 by CHP and boiler as shown by (57)-(58) [25]. In order to having a proper performance of P2G, each 2.7 kg of CO_2 is combined with 0.5 kg of H_2 to make 1 kg of CH4. Thus CO_2 to Hydrogen ratio is 5.3 The water electrolyzer unit consumes 0.05MWh to produce 1 kg of Hydrogen [13]. These constraints are modelled by (59)-(62).

$$CO2_{P2G}^{se,f,s,t} = CO2_{cap}^{se,f,s,t} - FR_{co2s}^{se,f,t} - FR_{sell}^{se,f,s,t} \tag{56}$$

$$CO2_{cap}^{se,f,s,t} \leq CO2_{chp\&bo}^{se,f,s,t} \tag{57}$$

$$CO2_{chp\&bo}^{se,f,s,t} = \left(P_{chp}^{se,f,t} / \eta_P^{chp} + H_{chp}^{se,f,t} / \eta_H^{chp} + H_{bo}^{se,f,s,t} / \eta_H^{bo} \right) .\alpha \tag{58}$$

$$CO2_{P2G}^{se,f,s,t} = 5.4 FR_{H2}^{se,f,s,t} \tag{59}$$

$$CO2_{P2G}^{se,f,s,t} = 2.7 G_{P2G}^{se,f,s,t} \tag{60}$$

$$P_{we}^{se,f,s,t} = 0.05 FR_{H2}^{se,f,s,t} \tag{61}$$

$$G_{in}^{se,f,s,t} + G_{P2G}^{se,f,s,t} - FR_{gs}^{se,f,t} = (P_{chp}^{se,f,t} / \eta_P^{chp} + H_{chp}^{se,f,t} / \eta_H^{chp} + H_{bo}^{se,f,s,t} / \eta_H^{bo}).\beta^{-1} \tag{62}$$

G. EV charging station modelling

The vehicle entrance pattern to the charging stations is usually achieved from the historical data. In this paper, it is assumed that each EV can stay in the station from 15 minute to 1 hour and station operator can charge or discharge the EV at each time interval (15 minute). Finally, the EV leaves the station fully or partially charged. The vehicle owner may receive an incentive in case of leaving with partial charge (this is the penalty cost for station operator). The station decision variables such as stopping time in station, charging time and rate, discharging time and rate and amount of stored energy in EV battery are optimized. The vehicle available in the charging station is expressed by (63). Equation (64) expresses charging and discharging power rate. The stored energy in EV is presented by (65) and (66). The vehicle energy is limited by (67) and amount of energy stored at leaving time is expressed by (68). The details of EV charging station modelling can be found in [26].

$$z_{vn}^{se,f,t+1} \leq z_{vn}^{se,f,t} \tag{63}$$

$$-P_{vn}^{\max} .z_{vn}^{se,f,t} \leq P_{vn}^{se,f,t} \leq P_{vn}^{\max} .z_{vn}^{se,f,t} \tag{64}$$

$$E_{vn}^{se,f,t} = P_{vn}^{se,f,t} .\Delta t \tag{65}$$

$$E_{vn}^{se,f,t+1} = E_{vn}^{se,f,t} + P_{vn}^{se,f,t+1} .\Delta t \tag{66}$$

$$E_{vn}^{se,f,t} \leq cap_{vn} \tag{67}$$

$$E_{vn}^{se,f,t_{leave}} = \psi_{vn}^{se,f,t} .cap_{vn} \tag{68}$$

H. Fault modelling

For resilience assessment, nine various faults are considered in each season. The faults are listed in Table II. In each season, there are nine faulty days and rest of the days are healthy days (Fault1). Faults 2 and 3 occur due to electrical network outage. The applied faults (i.e., events or outages) are typical and the system operation is not a function of fault type, time or location.

TABLE II: FAULTS SPECIFICATIONS

Fault No	Fault occurrence time periods				Fault modeling
	Spring	Summer	Autumn	Winter	
1	Without fault				Safe operation
2	68-85	48-65	70-96	1-31	$P_{in}^{se,f,s,t} = Q_{in}^{se,f,s,t} = 0$
3	24h	24h	24h	24h	
4	39-64	25-40	63-79	17-33	$P_{pv}^{se,f,s,t} = P_w^{se,f,s,t} = 0$
5	24h	24h	24h	24h	
6	70-89	77-96	3-18	74-96	$P_{chp}^{se,f,t} = Q_{chp}^{se,f,t} = H_{chp}^{se,f,t} = 0$
7	24h	24h	24h	24h	
8	1-30	1-10	1-8, 81-96	1-25, 74-96	$H_{bo}^{se,f,s,t} = 0$
9	24h	24h	24h	24h	
10	83-96	13-23, 63-82	16-24, 66-96	18-29, 63-91	$G_{in}^{se,f,s,t} = 0$

Disconnection of solar PV and wind units from network due to natural disasters are expressed by faults 4 and 5. CHP shutting down because of periodic maintenance is modelled by faults 6 and 7, boiler shutting down due to boiler repair is defined by faults 8 and 9 as well as fault 10 expresses natural gas network outage. In the proposed model, all the equations are important and some equations may not be regarded as the main ones. The proposed framework is modeled by combination of all formulas. The final optimization model is expressed as follows:

Minimizing Equation (1)

Subject to

Equations (2) to (68)

This article has been accepted for publication in a future issue of this journal, but has not been fully edited. Content may change prior to final publication. Citation information: DOI 10.1109/TII.2021.3121333, IEEE Transactions on Industrial Informatics

V. Case Study

The proposed microgrid is shown in Fig. 4. The nominal power of solar water heater 0.03 MW. The output power of solar PV panels can be expressed by (69) [27].

$$P_{PV}^{t} = \eta_{in} . N_k . P_{STC} . \frac{I_t}{I_{STC}} . \left(1+0.005.(T_t - 25)\right) \tag{69}$$

The set of PV array is composed by 6 pieces of solar panels. The rated power and area of one solar panel is about 250 W and 1.6 m^2, respectively. The rated power and area of PV array is 1.5 MW and 9.6 m^2. The other renewable resource is horizontal axis wind turbine. The output power of wind unit can be formulated as a function of wind speed shown by (70) [28].

$$P_w^t = \begin{cases} 0 & \upsilon_t \le \upsilon_{in}, \upsilon_t \ge \upsilon_{out} \\ \dfrac{\upsilon_t - \upsilon_{in}}{\upsilon_r - \upsilon_{in}} & \upsilon_{in} \le \upsilon_t \le \upsilon_r \\ P_r & \upsilon_r \le \upsilon_t \le \upsilon_{out} \end{cases} \tag{70}$$

Based on the wind speed and structure of turbine, it is assumed that the nominal power of wind turbine is equal to 1.5MW. The energy generation profile of renewable resources and loads in each season is shown by Fig. 6. The hourly price of active and reactive power and natural gas [19] is depicted in Fig. 7. The Efficiency of battery converter is 96% and the efficiency of other AC/DC converters is equal to 100%. The microgrid devices characteristics and conversion coefficients and economic parameters are given in Tables III and IV, respectively [12, 13, 20, 25, 26]. Some data are directly taken from the mentioned references but some other data are taken and then normalized according to range and scale of current test network. The numbers of seasons days equal 90, 93, 90 and 92 [19]. The daily time is modeled by 96 time-intervals each one 15 minute.

Every uncertain parameter follows a PDF with known mean and standard deviation. The standard deviation of uncertain parameters is considered by 10% and mean of these parameters is shown by Fig. 6. The PDF related to each uncertain parameter is approximated by 3 steps as discrete Gaussian PDF that are denoted as α, β, δ with probability equal to 0.06, 0.9 and 0.04, respectively. Amount of β is equal to mean and amount of α and δ are equal to 0.5 β, 1.5 β, respectively. The stochastic programming based on the scenario generation and scenario reduction techniques is used to handle the scenarios and uncertainty [29].

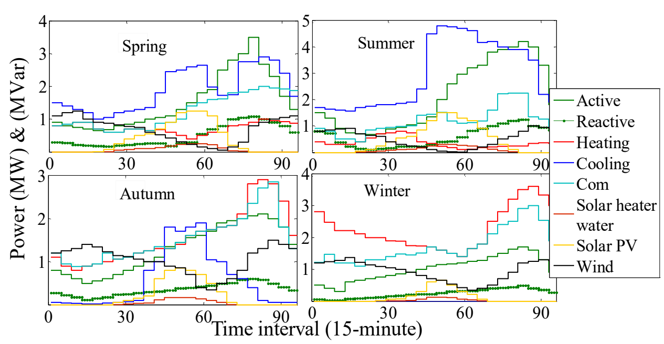

Fig. 6: Daily energy demands by loads and generated energy by renewables

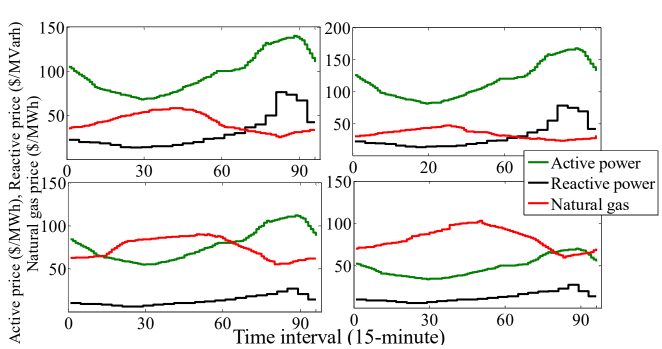

Fig. 7: Hourly price of active-reactive powers and natural gas for 4 seasons

TABLE III: Microgrid devices characteristics

Hybrid battery- capacitor storage	Heating storage	Cooling storage	CO_2 and natural gas storages
E_{es}^{ini}=0	E_{hs}^{ini}=0	E_{cs}^{ini}=0	M_{CO2s}^{ini}=0
E_{es}^{max}=3.8	E_{hs}^{max}=2.8	E_{cs}^{max}=1.8	M_{CO2s}^{max}=5000
E_{es}^{min}=0	E_{hs}^{min}=**0**	E_{cs}^{min}=**0**	M_{CO2s}^{min}=0
$P_{es,ch}^{max}$=0.8	$H_{hs,ch}^{max}$=0.8	$C_{cs,ch}^{max}$=0. 7	FR_{CO2s}^{max}=800
$P_{es,dis}^{max}$=0.9	$H_{hs,dis}^{max}$=0.8	$C_{cs,dis}^{max}$=0. 8	M_{gs}^{ini}=0
Q_{es}^{max}=0.3	η_{hs}^{ch}=0.98	η_{cs}^{ch}=0.97	M_{gs}^{max}=3000
η_{es}^{ch}=0.96	η_{hs}^{dis}=0.98	η_{cs}^{dis}=0.95	M_{gs}^{min}=**0**
η_{es}^{dis}=0.96	δ_{hs}^{self}=0.02	δ_{cs}^{self}=0	FR_{gs}^{max}=500
δ_{es}^{self}=0.01	η_{cs}^{ch}=0.97	COP_{cs}=3.5	
Chillers	**CHP**	**Boiler**	**EV**
COP_{ac}=1.2	η_p^{chp}=0.45	H_{bo}^{max}=2.1	P_{vn}^{max}=0.362
COP_{ec}=4	η_h^{chp}=0.5	η_h^{bo}=0.9	cap_{vn}=0.1

TABLE IV: Conversion coefficients and economic parameters

α(kg/MWh)	β(MWh/kg)	ξ_p	P_{CO2}($/kg)	P_{st}($)	P_{sh}($)	P_{sell}($/kg)
230	0.015	1.2	0.003	10	10	0.025

VI. Simulation Results

The problem is solved by a personal computer with processor core i7, CPU@ 4GHz, and RAM 8GB. The numerical results are given using GAMS software. In order to demonstrating the capability of the proposed model, the simulation is performed under four cases. The classifications of the cases are listed in Table V and case 4 is the final desired case. The primary network defined in Table V consists of electrical and natural gas networks, loads, CHP, boiler, wind, solar PV, solar water heater, electrical-absorption chillers, and EV charging station.

A. *Analysis of different cases*

The annual costs of different cases are shown by Table VI. The active power cost in case 4 is increased due to P2G operation and H_2 generation. Case 2 shows that the multi-type energy storage reduces the cost of purchased reactive power by 69.5%. The V2G operation and partial charge capability of EVs in the charging station reduce the load shedding cost by 6.5 % in case 3. In case 4, application of CCS and P2G reduces CO_2 emission and cost of natural gas by 75% and 6.1%, respectively.

B. *Resilience analysis*

The supplied load over the fault duration is the resilience index of current work that must be maximized. This index is integral of system performance function over the fault duration that is modelled by a nonlinear parameter in [30, 31]. For resilience analysis of the cases, the supplied load under fault condition is shown in the Fig.8. In Fig. 8-a, the fault occurs at time interval 48 to 65 and it is clear that not only the supplied electrical load by case 4 is improved by 96% but also 100% of load is supplied at time period between 50 to 60. Among all cases, case 4 has the best operation. Fig. 8-b demonstrates the supplied electrical load under fault 3 for different cases. Case 4 postpones the network deterioration for 3 hours, increases the electrical load supply by 150% at time intervals between 60 to 96, and improves the minimum load supply by 48%. The supplied heating load under fault 10 is shown in the Fig. 8-c. According to this figure, case 4 can supply 100% of heating load under first outage and the network degradation is postponed for 2.5 hours under second outage.

C. *Analysis of microgrid behavior under proposed case*

Comparing cases 1 and 4 shows that in case 4, the full cost is decreased by 8.2%, the emission, load shedding, and purchased natural gas costs are decreased by 75%, 19.3%, and 6.7%. In case 4, the adequacy, robustness and resilience of network are increased by 150%, 48% and 3 hours. Therefore, case 4 is considered as final case to be evaluated.

1) *Combinational load supply*

The price of electrical energy is high in spring-summer and the price of natural gas is high in autumn-winter. It is therefore expected that the combinational load be supplied by electrical power in autumn-winter and by heating power in other seasons. This point is confirmed in Fig. 9.

2) *Analysis of EV charging station under fault condition*

In proposed approach, the charging station is able to charging the EVs partially rather than fully and then it pays the penalty cost to EVs owners.

This article has been accepted for publication in a future issue of this journal, but has not been fully edited. Content may change prior to final publication. Citation information: DOI 10.1109/TII.2021.3121333, IEEE Transactions on Industrial Informatics

It is expected that such operation be utilized only when the grid electricity is in short supply. According to Table II, the system under faults 2 and 3 has electrical power shortage, it is therefore expected that the charging station accept the penalty cost and use the partial charge option. The numbers of EVs with partial and fully charges are depicted in Fig. 10. According to this figure, the partial charge occurs only under faults 2 and 3 and the EVs are fully charged under other faults. The penalty cost is a coefficient of electricity price and it is high in summer. As a result, 100% of the EVs are fully charged in summer under all faults but in the autumn and winter, 34% and 11% of EVs are fully charged.

TABLE V: CLASSIFICATIONS OF CASES

Case studies	Primary system	Natural gas storage	Heating, cooling and hybrid storages	V2G and Partial charge for EV	CO_2 storage	P2G and CO2 selling
Case 1	✓	✓	×	×	×	×
Case 2	✓	✓	✓	×	×	×
Case 3	✓	✓	✓	✓	×	×
Case 4	✓	✓	✓	✓	✓	✓

TABLE VI: ANNUAL OPERATION COST OF NETWORK UNDER DIFFERENT CASES

Various costs (\$/year)	Case 1	Case 2	Case 3	Case 4
Active cost	893368	886500	885516	966107
Reactive cost	76889	23483	23489	23478
Natural gas cost	1949473	1944768	1938149	1818667
Emission cost	34296	34288	34221	8496
CHP cost	7180	7360	7360	5720
Load shedding cost	36881	32837	30718	29754
EV partial charge cost	0	0	5565	4881
selling CO_2	0	0	0	106281
Full Cost	2998090	2929239	2925021	2750822

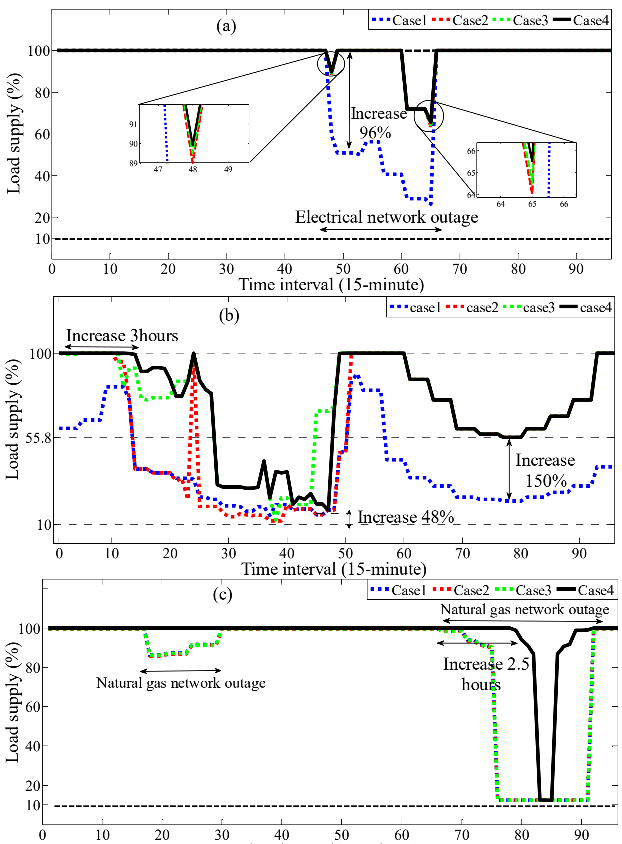

Fig. 8: Hourly supplied electrical load in fault 2 (a) and fault 3 (b) in summer and heating load in fault 10 (c) in winter under different cases

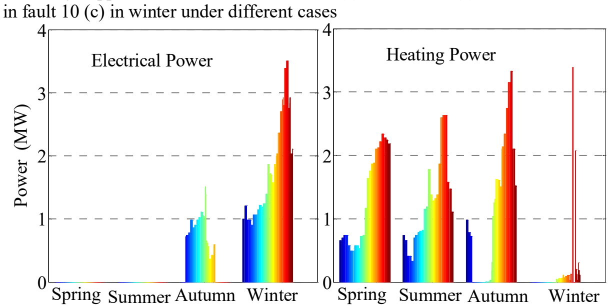

Fig. 9: Combinational load supply in four seasons

Figure 11 indicates the number of vehicles available in the charging station under fault 2 and without fault. The fault occurs from 0 to 31 time-periods. Under the fault, the station charges the vehicles rapidly and sends them out and do not operate the vehicles in V2G mode because the network is under fault and the power of the grid is required to supply the loads (the critical loads are in priority to be supplied). As a result, the vehicles are charged partially and leave the station. After fault, both the curves (with and without fault) fit each other and the station utilizes the vehicles in V2G mode. The duration of stay of vehicles in the station is increased to take part in energy management and peak load shaving.

3) *Heating and battery storages*

The heating demand is very high in autumn-winter and the network operation will be expensive under boiler outage; because not only the CHP generation is limited to the operation region but also price of natural gas to supply CHP in winter is high. The heating storage can fix this issue. The heat exchange of heating storage tank under fault 8 in autumn-winter is shown in the Fig. 12. Under the fault condition, the heat storage tank supplies the heating demand and reduces the network cost and CO_2 emission.

The battery storage with charging at low demand and discharging in peak demand shaves the peak load and reduces the cost. As seen in the Fig. 13, the battery not only is charged and discharged under low and peak demands but also is discharged under fault period and significantly reduces the unsupplied loads and penalty costs.

4) *Analysis of CO_2 capture, storage and trading*

Hourly generated CO_2 by CHP and boiler and captured CO_2 for CO_2 storage and P2G unit in winter under fault 10 (worst scenario) is shown in the Fig. 14-a. As seen in this figure, only 91 kg of CO_2 is released into the air at time interval 1 and at other time intervals all of the generated CO_2 is captured. Under other time periods, all of the generated CO_2 is captured in order to storing or supplying the P2G unit or selling CO_2. At time intervals 1 to 20 and 45 to 96, all captured CO_2 is stored in CO_2 storage tank. The P2G unit is turned on at time intervals 22 to 44 for natural gas regeneration. The CO_2 needed for P2G at time intervals 23 to 41 is summation of captured CO_2 and released CO_2 from storage tank as shown in the Fig. 14-b. The stored CO_2 is sold to \$175 in time intervals 87 to 90 and 96, and CO_2 storage tank becomes empty for next day. Fig. 14-c shows the CO_2 flow rate in order to selling CO_2 in 24h.

5) *Natural gas analysis*

In winter, the heating demand and price of natural gas are high, thus the natural gas network outage can be very risky and expensive for network management. The purchased natural gas from the gas network, stored gas, and delivered gas, and the regeneration of natural gas in winter under fault 10 is depicted in Fig. 15.

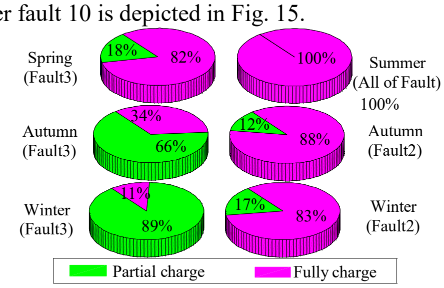

Fig. 10: EV with partial or full charge in four seasons under fault 2 and 3

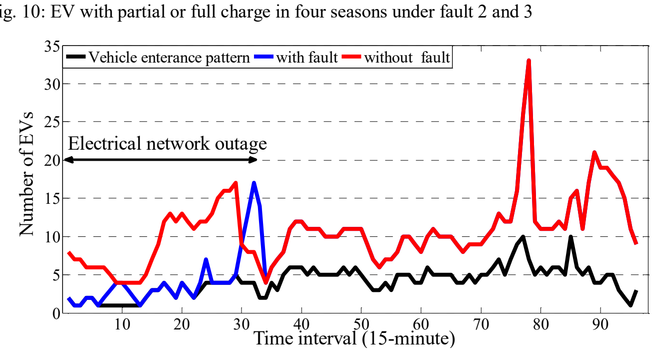

Fig. 11: Vehicle entrance pattern to charging station and hourly number of EV inside station with-without fault in winter

This article has been accepted for publication in a future issue of this journal, but has not been fully edited. Content may change prior to final publication. Citation information: DOI 10.1109/TII.2021.3121333, IEEE Transactions on Industrial Informatics

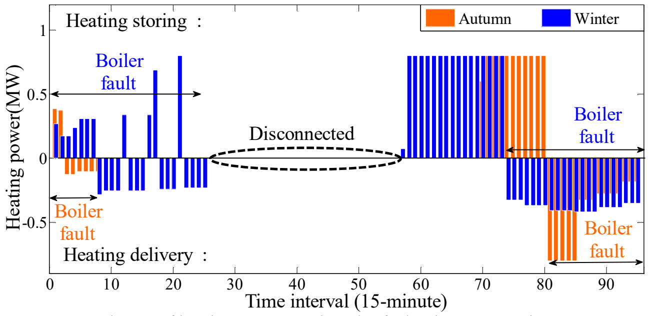

Fig. 12: Heat exchange of heating storage tank under fault 8 in autumn-winter

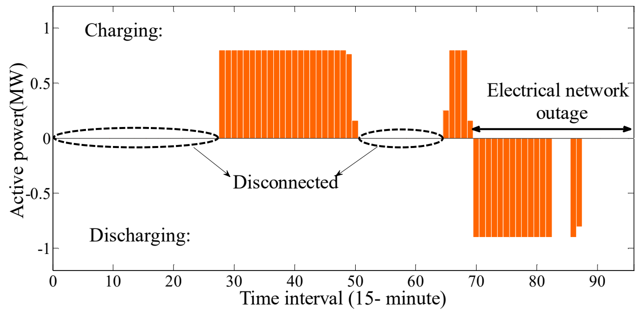

Fig. 13: Active power exchange of battery under fault 2 in autumn

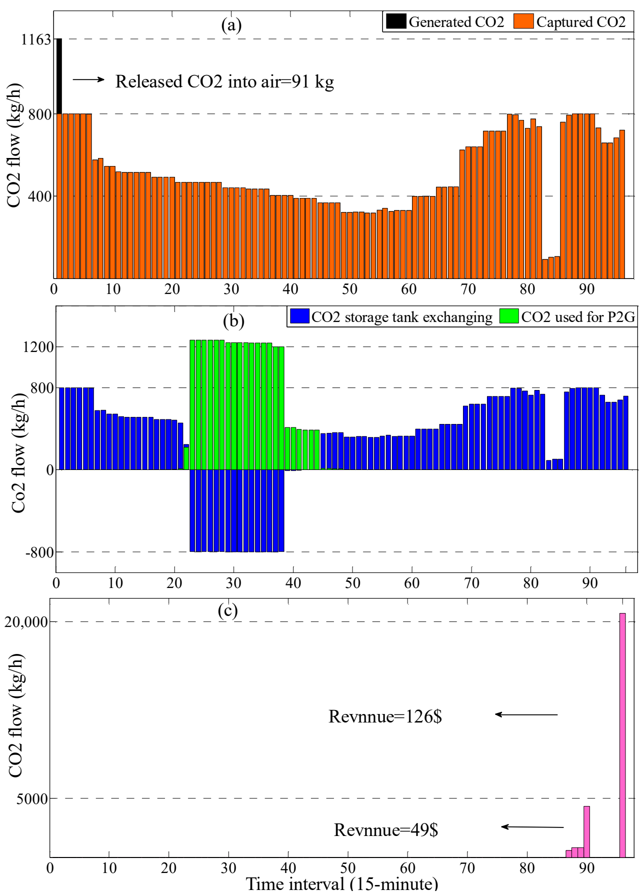

Fig. 14: Hourly generated and captured CO_2 (a), CO_2 storage tank exchanging and CO_2 used for P2G (b), CO_2 selling (c) in winter under fault 10

As seen in the figure, under first outage (time intervals 18 to 29), the natural gas needed by network is supplied by natural gas storage tank and P2G unit. Under second outage (time intervals 63 to 91), the natural gas needed by the network is supplied by natural gas storage tank. Therefore, not only lower cost is used to purchase the natural gas but also the network resilience is increased and CO_2 emission is decreased. The generated natural gas by P2G unit in four seasons under all faults is shown in the Fig. 16. As seen in this figure, in spring and autumn the P2G is turned on only under fault 3 because the electricity price is low and the network is facing electricity shortage.

The CHP therefore produces electricity and the required natural gas of CHP is supplied by P2G. In summer, the electricity price for water electrolyzer is high and the heating demand is low and P2G has no generation because the system does not need extra gas. In winter, the electricity price for water electrolyzer is low and the heating demand is high. As seen in the figure, under all faults except fault 3, P2G produces natural gas for boiler and CHP. Under fault 3, the CHP is not required to produce electricity and P2G operation is negligible. Because of P2G operation, the emission cost, the natural gas cost and the un-supplied load penalty cost are decreased by 75%, 6.1% and 3.1%, respectively.

6) *Analysis of CHP behavior*

The CHP operating points under all four seasons and the CHP operation region are depicted in Fig. 17. As seen in this figure, due to high price of electricity and low price of natural gas in spring-summer, the CHP generates more electrical and thermal powers in the spring-summer compared to the other seasons. The CHP heating generation is utilized in the spring-summer in order to supply the cooling demand. The CHP heating power in four seasons under fault 8 is shown by Fig. 18. As seen in the figure, the CHP generates heating power in order to compensating the heating shortage almost under all fault periods. Thus, the un-supplied heating load is decreased as well as network resilience is increased.

D. *Uncertainty analysis*

The stochastic model is more resilient under load or generation variations compared to the deterministic plan. In order to show this point, the percentage of supplied load under different cases is calculated for both the deterministic and stochastic plans as listed in Table VII.

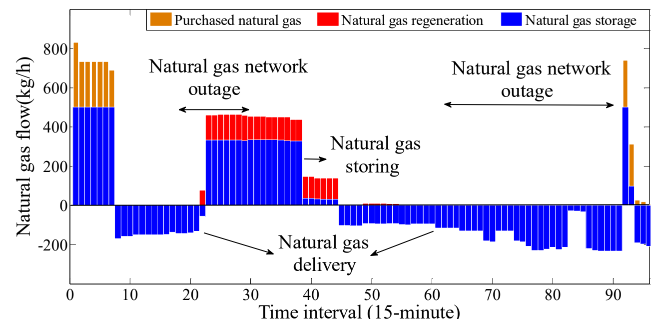

Fig. 15: Hourly purchased natural gas, natural gas regeneration and natural gas storage in winter under fault 10

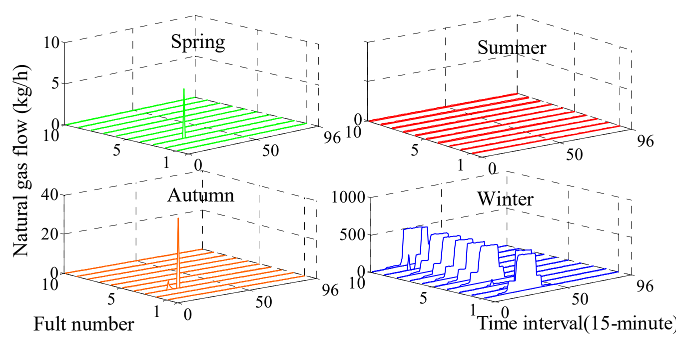

Fig. 16: P2G generation in four seasons under all of the faults

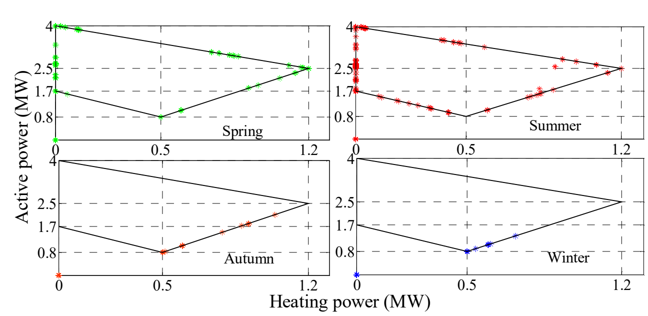

Fig. 17: CHP operating points under all four seasons and the CHP operation region

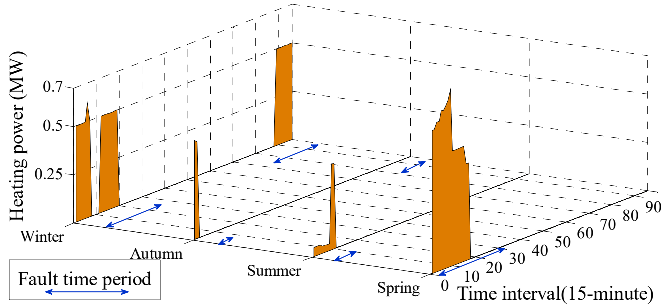

Fig. 18: CHP heating power in four seasons under fault 8

TABLE VII: PERCENTAGE OF LOAD SUPPLY UNDER DIFFERENT CASES

Case	Deterministic	Stochastic
A	66%	82%
B	55%	78%
C	47%	69%
D	39%	58%

Case A: Generation of wind and solar PV is decreased by 60%
Case B: Load increasing by 20%
Case C: Generation of wind and solar PV equal to zero
Case D: Load increasing by 20% and wind/solar generation equal to zero
The load supply under stochastic model is more than the deterministic plan in all cases. The annual cost of deterministic model is lower than the stochastic plan, but the resilience of network with stochastic plan is better. This point is the most important positive topic of uncertainty modelling especially for supplying the critical loads.

E. Uncertainty of EV charging behavior

The uncertainty of EV charging behavior is considered as vehicle entrance pattern and initial energy of EVs. The standard deviation of these parameters is considered by 10% (case 5) and 30% (case 6). Mean of vehicle entrance pattern is shown by Fig. 11 (black curve) and mean of initial EV energy is assumed equal to 25%. The results are listed in Table VIII.

TABLE VIII: ANNUAL COST UNDER DIFFERENT UNCERTAINTY CASES

Various costs ($/year)	Case 4	Case 5	Case 6
Active cost	966107	971221	971236
Reactive cost	23478	23478	23478
Natural gas cost	1818667	1818667	1818667
Emission cost	8496	8499	8499
CHP cost	5720	5728	5729
Load shedding cost	29754	29758	29758
EV partial charge cost	4881	4956	4958
Selling CO2	106281	106283	106285
Full Cost	2750822	2756024	2756040

Some costs such as active cost and CHP cost are changed, because the initial of EV in case 4 is constant but in cases 5 and 6 it is uncertain and needs more power from grid. As well, due to increasing CHP operation, the CO_2 emission (emission cost) is increased. The full cost in cases 5 and 6 is increased by 0.18% and 0.19%, respectively. Due to consideration of many uncertain parameters in the model such as behavior of renewables and loads, the EVs uncertainty has trivial effect on the system.

F. Demand response program

An incentive-based demand response program is modelled by shifting the electrical load to the other times. The range of shiftable load at each time is expressed by (71). The shifted load is added at next times as shown by (72). The final amount of demand is defined by (73). The demand response cost is calculated by (74) that should be added to the objective function.

$$DRP_{up}^{se,f,s,t} \le \gamma . L_{ea}^{se,f,s,t} \quad , DRP_{down}^{se,f,s,t} \le \gamma . L_{ea}^{se,f,s,t} \tag{71}$$

$$\sum_{t\in T} DRP_{up}^{se,f,s,t} = \sum_{t\in T} DRP_{down}^{se,f,s,t} \tag{72}$$

$$PD_{DR}^{se,f,s,t} = L_{ea}^{se,f,s,t} + DRP_{up}^{se,f,s,t} - DRP_{down}^{se,f,s,t} \tag{73}$$

$$C_{DR} = \sum_{se\in SE}\left(\sum_{f\in F} D_{se}^{f}\left(\sum_{s\in SC}\left(\sum_{t\in T} p_{pin}^{se,t}\cdot pr_{drp}^{se,f,s,t}\left(DRP_{up}^{se,f,s,t}+DRP_{down}^{se,f,s,t}\right)\cdot\right).pro_s\right)\right) \tag{74}$$

The results including demand responsive loads are shown in Table IX. The purchased cost of active power is reduced significantly, because the load supply cost under on-peak is reduced. Therefore, the annual operational cost is reduced by 0.6 %.

TABLE IX: ANNUAL OPERATION COST WITH AND WITHOUT DRP

Various costs ($/year)	Without DRP	With DRP
Active cost	966107	952181
Reactive cost	23478	23480
Natural gas cost	1818667	1818658
Emission cost	8496	8492
CHP cost	5720	5716
Load shedding cost	29754	2953
EV partial charge cost	4881	4881
Selling CO2	106281	106088
DRP cost	0	23785
Full operation cost	2750822	2734058

G. Natural gas price analysis

In this paper, the gas price is considered different under off-peak and on-peak time-periods, but the gas price may be constant due to natural gas inertia. In order to show the impacts on gas price on the model, the system is simulated under two cases including constant (39$/MWh) and variable (the proposed cost) natural gas price. The results are listed in Table X. The final cost with content gas price is increased by 0.05%. As a result, the natural gas inertia has a small effect on the results.

TABLE X: ANNUAL OPERATION COST OF NETWORK UNDER CONSTANT AND VARIABLE NATURAL GAS PRICE

Costs ($/year)	Variable price	Constant price
Active power	966107	966212
Reactive power	23478	23463
Natural gas	1818667	1819921
Emission	8496	8500
CHP	5720	5723
Load shedding	29754	29755
EV partial charge	4881	4881
selling CO2	106281	106288
Final Cost	2750822	2752167

H. Battery, electrolyzer and methanation operational cost

The operational cost of electrolyzer, methanation and battery are often high and the fast action reduces their lifetime. In order to show the effects of such costs on the system, the operational costs of battery, electrolyzer, methanation are considered as 100 $/MWh, 80 $/Kg, 140 $/Kg, respectively [32] with life time equal to 5 years. Such costs increase the annual cost of system to 2,874,129 $ which shows 4.5% increment. Therefore, considering the operational cost for the devices with fast operation like battery, electrolyzer and methanation increases the accuracy of the outputs.

VII. CONCLUSION

This paper modeled a multi-carrier energy hub in the microgrid. The natural gas, electricity, heating, cooling, H_2, CO_2, and renewables were included in the model. The microgrid utilized multiple resources and capacities. A hybrid electrical storage, thermal storage, EV charging station, P2G system, CCHP, and CCS were coordinated in the given model. Different faults and events were modeled in all seasons to evaluate the energy resilience. Various cases were implemented, simulated and studied. The results confirmed that the multi type energy storages decreased the cost by 69.5%. The EV charging station can reduce the load shedding cost by 6.5 %. The CCS captures about 75% of CO_2 emission. The P2G reduced the natural gas cost by 6.1%. The proposed case including all resources at the same time (case 4) decreased the total system cost by 8.2%. The proposed model reduced the emission, load shedding and gas cost by 75%, 19.3%, and 6.7%, respectively.

In the proposed case, CO_2 trading was considered and the annual revenue from CO_2 selling was 126986 $. The optimal coordination of multi type storages, CHP, boiler and P2G made positive economic and technical impacts on the system, where the costs were reduced and the resilience, adequacy, and robustness were improved.

REFERENCES

[1] W. Gu, Z. Wang, Z. Wu, Z. Luo, Y. Tang, and J. Wang, "An online optimal dispatch schedule for CCHP microgrids based on model predictive control," *IEEE Transactions on Smart Grid,* vol. 8, no. 5, pp. 2332-2342, 2016.

[2] H. R. Galiveeti, A. K. Goswami, and N. B. D. Choudhury, "Impact of plug-in electric vehicles and distributed generation on reliability of distribution systems," *Engineering Science and Technology, an International Journal,* vol. 21, no. 1, pp. 50-59, 2018.

[3] Y. Li, Z. Li, F. Wen, and M. Shahidehpour, "Minimax-regret robust co-optimization for enhancing the resilience of integrated power distribution and natural gas systems," *IEEE Transactions on Sustainable Energy,* vol. 11, no. 1, pp. 61-71, 2018.

[4] Y. Cao, W. Wei, J. Wang, S. Mei, M. Shafie-khah, and J. P. Catalão, "Capacity planning of energy hub in multi-carrier energy networks: a data-driven robust stochastic programming approach," *IEEE Transactions on Sustainable Energy,* vol. 11, no. 1, pp. 3-14, 2018.

[5] A. Ghasemi, M. Banejad, and M. Rahimiyan, "Integrated energy scheduling under uncertainty in a micro energy grid," *IET Generation, Transmission & Distribution,* vol. 12, no. 12, pp. 2887-2896, 2018.

[6] S. Kuravi, J. Trahan, D. Y. Goswami, M. M. Rahman, and E. K. Stefanakos, "Thermal energy storage technologies and systems for concentrating solar power plants," *Progress in Energy and Combustion Science,* vol. 39, no. 4, pp. 285-319, 2013.

[7] M. Rastegar, M. Fotuhi-Firuzabad, H. Zareipour, and M. Moeini-Aghtaieh, "A probabilistic energy management scheme for renewable-based residential energy hubs," *IEEE Transactions on Smart Grid,* vol. 8, no. 5, pp. 2217-2227, 2016.

[8] S. Mahdavi, R. Hemmati, and M. A. Jirdehi, "Two-level planning for coordination of energy storage systems and wind-solar-diesel units in active distribution networks," *Energy,* vol. 151, pp. 954-965, 2018.

[9] Y. Cheng, N. Zhang, B. Zhang, C. Kang, W. Xi, and M. Feng, "Low-carbon operation of multiple energy systems based on energy-carbon integrated prices," *IEEE Transactions on Smart Grid,* vol. 11, no. 2, pp. 1307-1318, 2020.

[10] G. Piperagkas, A. Anastasiadis, and N. Hatziargyriou, "Stochastic PSO-based heat and power dispatch under environmental constraints incorporating CHP and wind power units," *Electric Power Systems Research,* vol. 81, no. 1, pp. 209-218, 2011.

[11] V. Economics, "State and trends of carbon pricing 2017," 2017.

[12] H. Saboori and R. Hemmati, "Considering carbon capture and storage in electricity generation expansion planning," *IEEE Transactions on Sustainable Energy,* vol. 7, no. 4, pp. 1371-1378, 2016.

[13] H. Mehrjerdi, "Optimal correlation of non-renewable and renewable generating systems for producing hydrogen and methane by power to gas process," *International Journal of Hydrogen Energy,* vol. 44, no. 18, pp. 9210-9219, Apr. 2019.

[14] S. Clegg and P. Mancarella, "Storing renewables in the gas network: modelling of power-to-gas seasonal storage flexibility in low-carbon power systems," *IET Generation, Transmission & Distribution,* vol. 10, no. 3, pp. 566-575, 2016.

[15] Y. Li *et al.*, "Optimal stochastic operation of integrated low-carbon electric power, natural gas, and heat delivery system," *IEEE Transactions on Sustainable Energy,* vol. 9, no. 1, pp. 273-283, 2017.

[16] M. Amirioun, F. Aminifar, and H. Lesani, "Resilience-oriented proactive management of microgrids against windstorms," *IEEE Transactions on Power Systems,* vol. 33, no. 4, pp. 4275-4284, 2017.

[17] R. Zhang *et al.*, "Day-ahead scheduling of multi-carrier energy systems with multi-type energy storages and wind power," *CSEE Journal of Power and Energy Systems,* vol. 4, no. 3, pp. 283-292, 2018.

[18] Q. Xu, L. Li, X. Chen, Y. Huang, K. Luan, and B. Yang, "Optimal economic dispatch of combined cooling, heating and power-type multi-microgrids considering interaction power among microgrids," *IET Smart Grid,* vol. 2, no. 3, pp. 391-398, 2019.

[19] T. Ma, J. Wu, L. Hao, W.-J. Lee, H. Yan, and D. Li, "The optimal structure planning and energy management strategies of smart multi energy systems," *Energy,* vol. 160, pp. 122-141, 2018.

[20] T. Shekari, A. Gholami, and F. Aminifar, "Optimal energy management in multi-carrier microgrids: an MILP approach," *Journal of Modern Power Systems and Clean Energy,* vol. 7, no. 4, pp. 876-886, 2019.

[21] D. J. Olsen, N. Zhang, C. Kang, M. A. Ortega-Vazquez, and D. S. Kirschen, "Planning low-carbon campus energy hubs," *IEEE Transactions on Power Systems,* vol. 34, no. 3, pp. 1895-1907, 2018.

[22] J. Yang, N. Zhang, Y. Cheng, C. Kang, and Q. Xia, "Modeling the operation mechanism of combined P2G and gas-fired plant with CO2 recycling," *IEEE Transactions on Smart Grid,* vol. 10, no. 1, pp. 1111-1121, 2018.

[23] M. H. Amirioun, F. Aminifar, and M. Shahidehpour, "Resilience-promoting proactive scheduling against hurricanes in multiple energy carrier microgrids," *IEEE Transactions on Power Systems,* vol. 34, no. 3, pp. 2160-2168, 2018.

[24] T. Akbari and M. T. Bina, "A linearized formulation of AC multi-year transmission expansion planning: A mixed-integer linear programming approach," *Electric Power Systems Research,* vol. 114, pp. 93-100, 2014.

[25] T. Ma, J. Wu, and L. Hao, "Energy flow modeling and optimal operation analysis of the micro energy grid based on energy hub," *Energy Conversion and Management,* vol. 133, pp. 292-306, 2017.

[26] H. Mehrjerdi and R. Hemmati, "Electric vehicle charging station with multilevel charging infrastructure and hybrid solar-battery-diesel generation incorporating comfort of drivers," *Journal of Energy Storage,* vol. 26, pp. 100924, 2019.

[27] L. Xu, X. Ruan, C. Mao, B. Zhang, and Y. Luo, "An improved optimal sizing method for wind-solar-battery hybrid power system," *IEEE Transactions on Sustainable Energy,* vol. 4, no. 3, pp. 774-785, 2013.

[28] A. Soroudi, M. Aien, and M. Ehsan, "A probabilistic modeling of photo voltaic modules and wind power generation impact on distribution networks," *IEEE Systems Journal,* vol. 6, no. 2, pp. 254-259, 2011.

[29] M. Bornapour, R.-A. Hooshmand, A. Khodabakhshian, and M. Parastegari, "Optimal stochastic scheduling of CHP-PEMFC, WT, PV units and hydrogen storage in reconfigurable micro grids considering reliability enhancement," *Energy Conversion and Management,* vol. 150, pp. 725-741, 2017.

[30] Z. Wang, C. Shen, Y. Xu, F. Liu, X. Wu, and C.-C. Liu, "Risk-limiting load restoration for resilience enhancement with intermittent energy resources," *IEEE Transactions on Smart Grid,* vol. 10, no. 3, pp. 2507-2522, 2018.

[31] H. Gao, Y. Chen, S. Mei, S. Huang, and Y. Xu, "Resilience-oriented pre-hurricane resource allocation in distribution systems considering electric buses," *Proceedings of the IEEE,* vol. 105, no. 7, pp. 1214-1233, 2017.

[32] H. Mehrjerdi, "Dynamic and multi-stage capacity expansion planning in microgrid integrated with electric vehicle charging station," *Journal of Energy Storage,* vol. 29, pp. 101351, 2020.